Preliminary large-eddy simulations of flow around a NACA 4412 airfoil using unstructured grids

By Kenneth Jansen

1. Motivation and objectives

Large-eddy simulation (LES) has matured to the point where application to complex flows is desirable. The extension to higher Reynolds numbers leads to an impractical number of grid points with existing structured-grid methods. Furthermore, most real world flows are rather difficult to represent geometrically with structured grids. Unstructured-grid methods offer a release from both of these constraints. However, just as it took many years for structured-grid methods to be well understood and reliable tools for LES, unstructured-grid methods must be carefully studied before we can expect them to attain their full potential.

In the past two years, important building blocks have been put into place making possible a careful study of LES on unstructured grids. The first building block was an efficient mesh generator which allowed the placement of points according to smooth variation of physical length scales. This variation of length scales is in all three directions independently, which allows a large reduction in points when compared to structured-grid methods, which can only vary length scales in one direction at a time. The second building block was the development of a dynamic model appropriate for unstructured grids. The principle obstacle was the development of an unstructured-grid filtering operator. New filtering operators were developed in Jansen (1994). In the past year, some of these filters have been implemented into a highly parallelized finite element code based on the Galerkin/least-squares finite element method (see Jansen *et al.* (1993) and Johan *et al.* (1992)).

We have chosen the NACA 4412 airfoil at maximum lift as the first simulation for a variety of reasons. First, it is a problem of significant interest since it would be the first LES of an aircraft component. Second, this flow has been the subject of three experimental studies (Coles and Wadcock (1979), Hasting and Williams (1987), and Wadcock (1987)). The first study found the maximum lift angle to be 13.87°. The later studies found the angle to be 12°. Wadcock reports in the later study that the early data agree very well with his new data at 12°, suggesting that the early experiment suffered from a non-parallel mean flow in the Caltech wind tunnel. It should be pointed out that the Reynolds-averaged simulations are usually run at 13.87° and do not agree with the data when run at 12° as will be shown later in this study. It is hoped that LES can clarify this controversy. The third reason for considering this flow is the variety of flow features which provide an important test of the dynamic model. Starting from the nose where the flow stagnates, thin laminar boundary layers are formed in a very favorable pressure gradient. This pressure gradient soon turns adverse, driving the flow toward a leading edge separation. Only the onset of turbulence can cause the flow to remain attached or to reattach

if it did separate. The persistent adverse pressure gradient eventually drives the turbulent flow to separate in the last 20 percent of chord. The separation bubble is closed near the trailing edge as the retarded upper surface boundary layer interacts with the very thin lower surface boundary layer. The large difference in boundary layers creates a challenging wake to simulate. Only the dynamic model can be expected to perform satisfactorily in this variety of situations: from the laminar regions where it must not modify the flow at all to the turbulent boundary layers and wake where it must represent a wide variety of subgrid-scale structures.

The flow configuration we have chosen is that of Wadcock (1987) at Reynolds number based on chord $Re_c = u_\infty c/\nu = 1.64 \times 10^6$, Mach number $M = 0.2$, and $12°$ angle of attack.

2. Accomplishments

2.1 Dynamic model implemented and tested

The only obstacle to implementing a dynamic model on unstructured grids is extension of the filtering operator. Four filtering operators were proposed in Jansen (1994). Two of these models were implemented and compared using a simple analytic velocity field for which the filtered values can be determined exactly. From this test, the generalized top-hat was found to be the most accurate, and all subsequent calculations have been carried out using this filter.

2.2 Simulations

A series of simulations has been performed in the last year to develop experience with this new approach. The first simulation was intentionally very coarse as we hoped to improve the mesh selectively and develop an understanding of the sensitivity of the solution to the grid improvements.

2.2.1 First simulation

The first simulation was performed on a very coarse mesh. The near-wall grid did not attempt to resolve the near-wall layer accurately in the first 20 percent of chord and only marginally resolved the remaining flow ($\Delta_x^+ = 300$, $\Delta_z^+ = 80$) at the wall. The grid was coarsened in the streamwise and spanwise directions coming off the wall as suggested by Chapman (1979). The resulting coefficient of pressure distribution was reasonably well predicted on this mesh (see Fig. 1), but the velocity profiles showed poor agreement with the experiment.

2.2.2 Improvement of outer layer

Careful scrutiny of the mesh revealed that the strategy of coarsening in the streamwise direction coming off the wall was inappropriate at this Reynolds number. The inner-layer spacing, Δ, scales on wall units.

$$\frac{\Delta}{c} \propto \frac{\nu}{u_\tau c} = \frac{\sqrt{2}}{Re_c \sqrt{C_f}}$$

Here, ν, is the kinematic viscosity, c is the chord length, and u_τ is the friction velocity defined to be the square root of the coefficient of friction, C_f, over two.
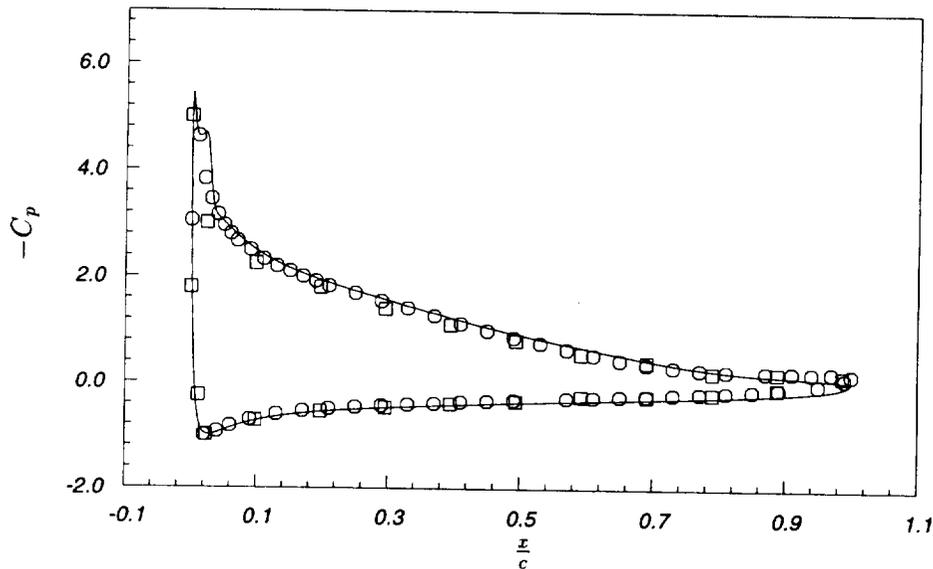
FIGURE 1. Coefficient of pressure along the airfoil surface. LES ———— , Hastings and Williams o , Wadcock (1987) □ .

The outer-layer spacing scales on the boundary layer thickness, δ_{99}. It is reasonable to expect the large eddies in the outer part of the boundary layer to be of order δ_{99}, and therefore the outer-layer spacing, in all directions, should never exceed

$$\Delta = \frac{\delta_{99}}{5}$$

By using Wadcock's experimental data for the C_f and δ_{99}, one can compare these two resolution restrictions as is done in Fig. 2. This figure contains three curves. The solid curve describes the variation of a 200 wall-unit spacing (which can be associated with the streamwise spacing near the wall) over the upper surface where the boundary layer is attached. The dashed curve describes the same variation of 50 wall units (which can be associated with spanwise spacing near the wall). The chain dash curve is the outer-layer spacing as described above. Several points can be made in this figure. First, all three curves change by over an order of magnitude from the tip to the tail region. This illustrates how an unstructured grid saves points by matching resolution to the local changes in the length scales in the streamwise direction. For example, a structured grid would be forced to carry the fine spanwise resolution required near the nose through the entire domain. Second, when comparing the near-wall spanwise resolution to the outer-layer resolution, it is clear that coarsening the spanwise resolution as the distance from the wall increases is justified. The final point, apparent from this figure, is that coarsening of the streamwise resolution in the outer layer is not justified. In fact, over much of the airfoil surface the outer-layer grid resolution is more restrictive than the
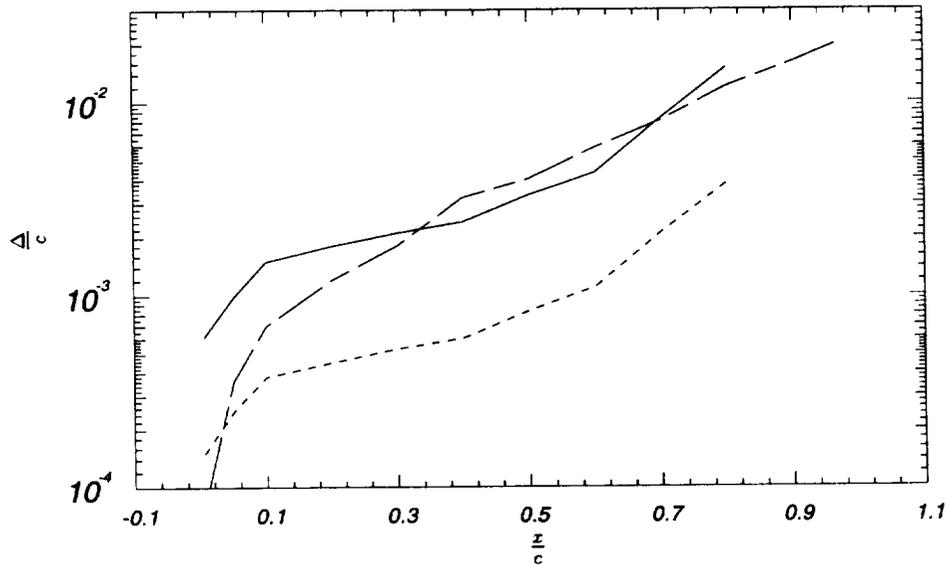
FIGURE 2. Comparison of length scales over the airfoil surface. 200 wall units (streamwise near-wall spacing) ——— , $\delta_{99}/5$ (outer-layer spacing) ———— , 50 wall units (spanwise near-wall spacing) ———— .

inner-layer resolution. The choices of 200 wall units and 5 points per boundary layer thickness are somewhat arbitrary, but they are believed to be comparable in their degree of coarseness. It is interesting to observe that the crossover between these two curves corresponds to $Re_\tau = (u_\tau\delta_{99}/\nu) = 1000$. Therefore, when above 1000, the inner-layer resolution is the most restrictive. Otherwise, the outer-layer resolution is the most restrictive. Only at higher Reynolds numbers will coarsening in the streamwise direction be justified.

Considering the above discussion, a new mesh was made where the coarsening of the streamwise spacing was delayed until outside of the boundary layer. This resulted in a mesh with nearly twice as many points as the previous simulation. It also resulted in a rather dramatic change in the early boundary layer structure. It seems that the improved resolution of the outer layer allowed a better resolution of the leading edge separation. The new simulation led to a train of spanwise coherent vortices. These vortices broke down into turbulence at about 10 percent of chord.

The persistence of the spanwise coherent vortices was not in line with the experiments which were all tripped. Some evidence as to the importance of the tripping can be seen in Fig. 3 where we compare the surface coefficient of pressure distribution from the free transition simulation to two experimental data sets from Hastings and Williams (1987). The square data set was taken without a transition strip while the circle data set was taken with a transition strip. Our simulation shows rather good agreement with the free transition. Unfortunately, all velocity and Reynolds stress data were taken with the transition strip in place and agreement with these
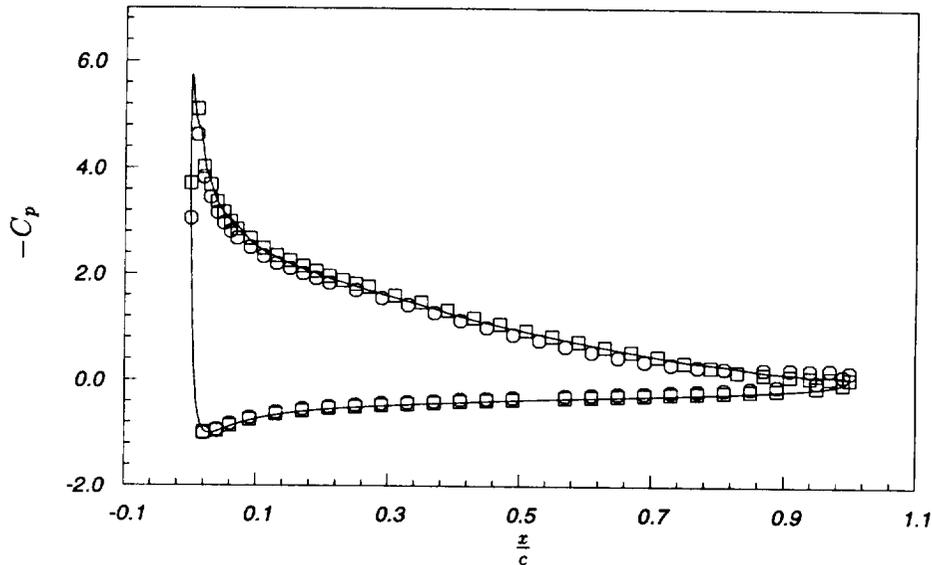
FIGURE 3. Coefficient of pressure along the airfoil surface. LES ———— , Hastings and Williams without trip □ , Hastings and Williams tripped ○ .

quantities is substantially worse than with C_p.

2.2.3 Grid refinement study of the nose

The dramatic change of the flow with changed resolution indicated a need for further refinement in the nose region. At the same time we also hoped to model the transition through a steady blowing pattern as shown in Fig. 4. A shape that could be easily resolved was chosen. Therefore, we could be certain that any sensitivity to grid refinement would be associated with the turbulence structures responding to the blowing and not the resolution of the blowing itself.

A new mesh was generated where the streamwise and spanwise resolution were improved by a factor of two everywhere on the upper surface. The normal spacing was improved at the wall by a factor of two as well, but this did not lead to a doubling of points in this direction due to the stretching. The spanwise domain was cut in half (from $0.05c$ to $0.025c$) for this simulation. Therefore, the number of points approximately doubled rather than a quadrupling.

There was again a rather dramatic change in the solution and so another mesh was generated. This mesh again improved the streamwise and spanwise resolution by a factor of two, although, this time, only in the first 5 percent of chord. The three surface meshes of the first 10 percent of chord are shown in Fig. 5. The velocity profiles in the first 5 percent of chord are shown in Fig. 6. For this forcing pattern, the flow is nearly spanwise- and streamwise-resolution independent.
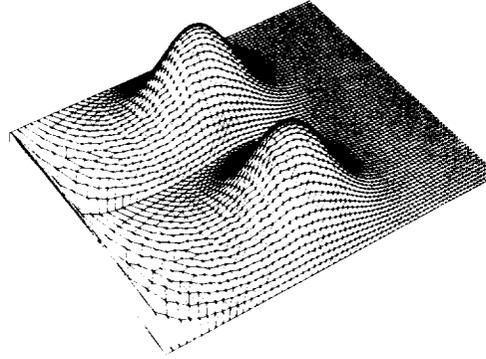
Kenneth Jansen

FIGURE 4.   Elevation plot of the steady jet normal to the airfoil surface. The actual grid is shown to confirm resolution.
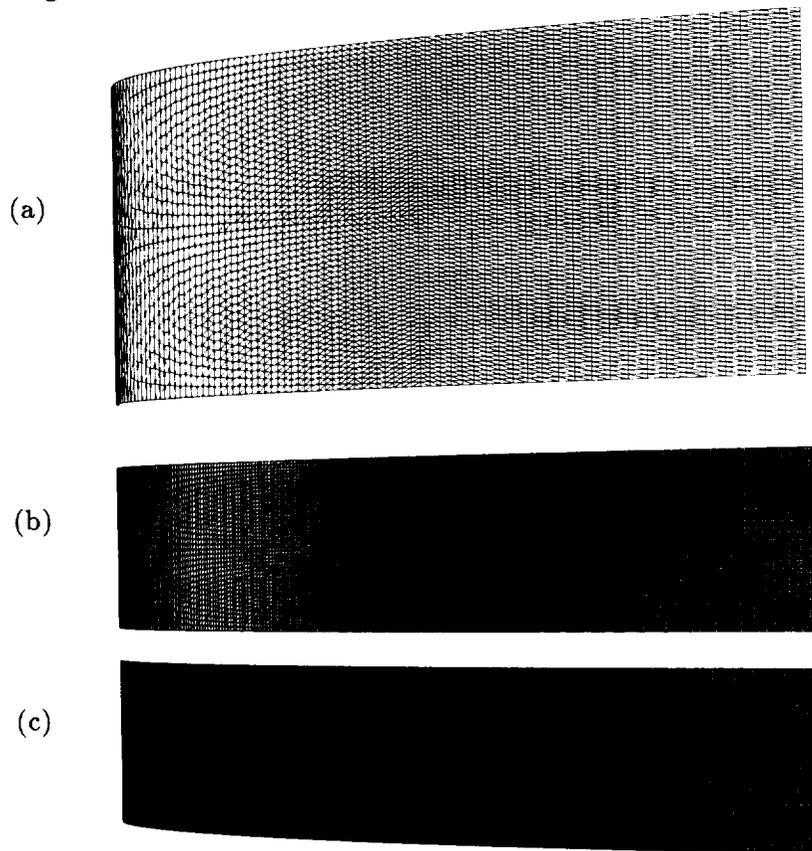
(a)

(b)

(c)

FIGURE 5.   Surface meshes near the leading edge $(0.0 < x/c < 0.1)$. Mesh (b) has been refined by a factor of 2, both spanwise and streamwise, from mesh (a). The spanwise domain is also halved. Mesh (c) has been refined by a factor of 2, both spanwise and streamwise, from mesh (b) in the first 5 percent of chord.
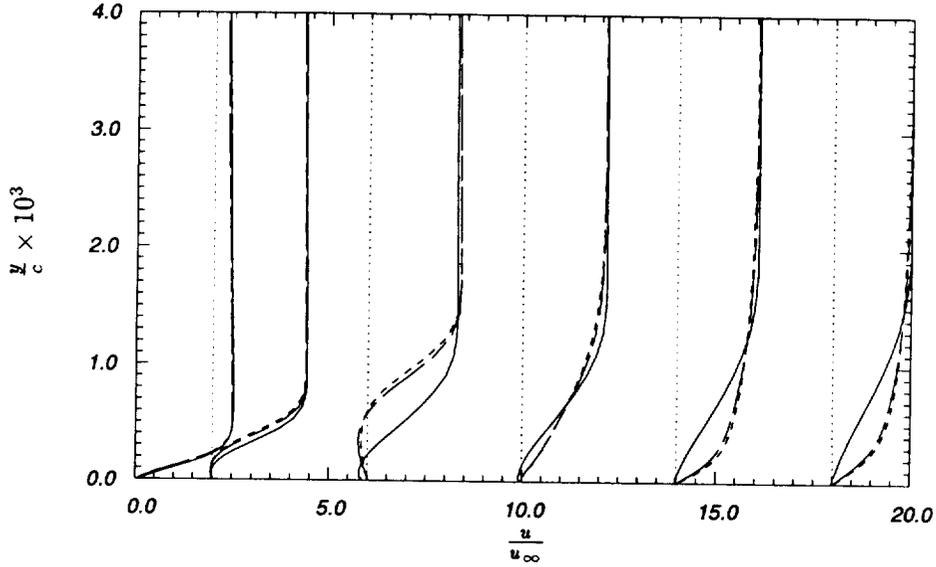
FIGURE 6. Profiles of tangential velocity component at various positions along the airfoil surface ($x/c = 0.005, 0.01, 0.02, 0.03, 0.04, 0.05$). Solutions correspond to grids from previous figure; mesh (a) ———— , mesh (b) —— — — , mesh (c) - - - - .
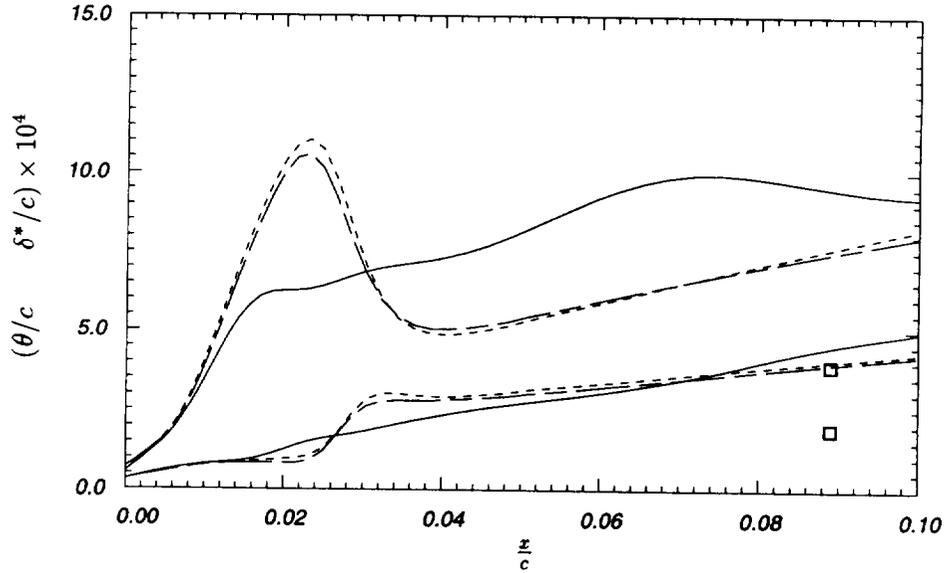

FIGURE 7. Boundary layer parameters (lower curves and data are momentum thickness (θ), higher curves and data are displacement thickness (δ^*)) along the airfoil surface. Solutions correspond to meshes from Fig. 5; mesh (a) ———— , mesh (b) —— — — , mesh (c) - - - - , Wadcock (1987) ($\square$).

2.3 More accurate transition

While it was useful to obtain a grid-independent solution at the forcing prescribed, the final solution does not agree with experiment, as can be seen in Fig. 7. Here, the momentum and displacement thickness of the grid-independent calculations can be seen to be substantially greater than the experiments at the first available datum point. The discrepancy seems to be associated with the laminar separation at 1 percent of chord. The simulation suggests a transition in the free shear layer, followed by a turbulent reattachment. This mode of transition seems to give the flow a large jump in momentum and displacement thickness. The experiment did not seem take this route to transition. For this reason a more careful study of transition is currently underway.

Wadcock used a strip of tape with serrations cut into the edge on the upstream side. The serrated tape can be modeled in a coarse fashion by our current simulation as can be seen in Fig. 8. The tape is effectively a forward facing step (with serrations) of height $\delta_{99}/4$, followed by a backward facing step. Calculations are underway with this modification.
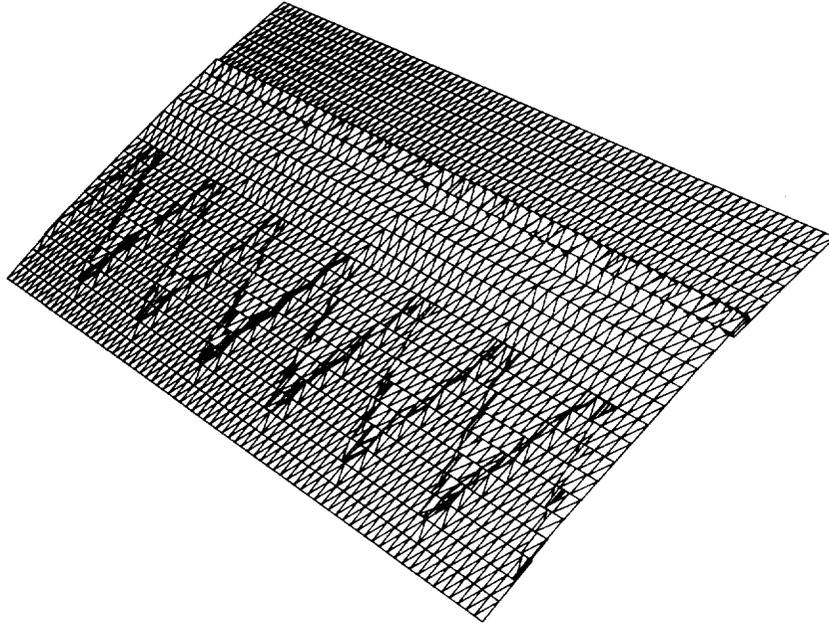

FIGURE 8.   A transition strip is modeled geometrically by applying a no-slip boundary condition to the nodes which form a surface of height, shape, and position equivalent to Wadcock's serrated tape which was applied to the airfoil surface.

2.4 Reynolds-averaged simulations

Reynolds-averaged Navier-Stokes simulations (RANS) have not shown good agreement with the experimental data. However, given the cost of LES, they can be a

helpful tool for suggesting sensitivity to changes of basic flow parameters since they require so little computational time. While the results are not expected to be quantitatively correct, trends can at least be suggested by RANS and later confirmed by LES.

A series of RANS calculations was performed to chart various trends in this flow. The RANS calculations used the commonly accepted NASA code (INS2D) of Rogers (1991) and employed a $k - \omega$ model from Menter (1994). First, the effect of angle-of-attack and wind tunnel walls are compared in Figures 9 and 10. The boundary condition on the wind tunnel walls is a slip condition. This accounts for the blockage of the walls without requiring resolution of the boundary layers on them. The effects are compared together because it is common among the RANS modeling community to adjust the angle-of-attack of free air calculations to account for the walls. Figure 10 suggests that the flattening of the C_p near the trailing edge (which is associated with the large separation there) is affected strongly by angle-of-attack and only weakly by the wind tunnel walls. The 13.87° angle-of-attack cannot be justified with the hope of accounting for the effects of the wind tunnel walls in free air calculations.

The second trend studied with the RANS code was the effect of transition position. When the RANS code was run with the transition point fixed at the position of Wadcock's strip, a leading edge separation developed on sufficiently fine meshes. Once beyond the transition point, the flow reattaches. This provides an independent verification of the results observed in the LES.

3. Future plans

3.1 Grid-independent solution of flow with a transition strip

The calculation using the transition strip described above will be continued and checked for grid dependence. It should be noted that grid independence can only be achieved beyond a short distance downstream of the transition strip. True grid independence of the strip and transition itself is probably too expensive to be practical, even with an unstructured grid. It may be necessary to provide small disturbances upstream of the strip to mimic the interaction of freestream turbulence with the strip. This capability has been implemented and tested in the code using a wall jet with spatial and temporal variation.

3.2 Inclusion of the wind tunnel walls

The RANS studies indicated a moderate effect of the wind tunnel walls on the solution. Future simulations will be done with a slip boundary conditions on the wind tunnel walls. Meshes have already been generated for this purpose as can be seen in Fig. 11.

3.3 Higher order methods

Given the number of points that are required to get a grid-independent solution, it seems clear that higher order methods should be explored. This is relatively easy, but non-trivial, to do with the finite element method. There are two benefits to higher order methods besides the obvious one of higher accuracy. First, the higher
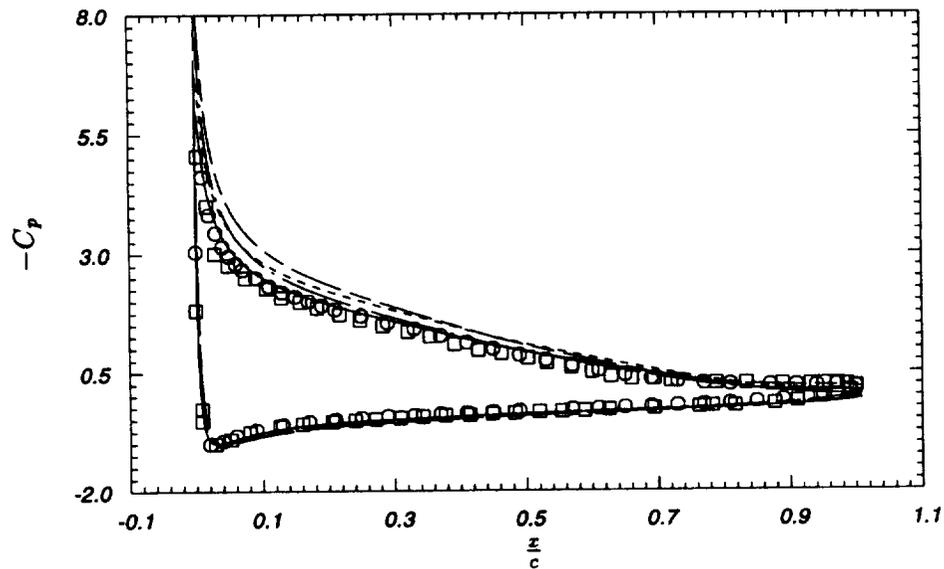
FIGURE 9.   Coefficient of pressure along the airfoil surface from RANS simulations. $12°$ in free air ——— , $12°$ with walls ---- , $13.87°$ in free air —·— , $13.87°$ with walls —--— , Hastings and Williams (1987) o , Wadcock (1987) □ .
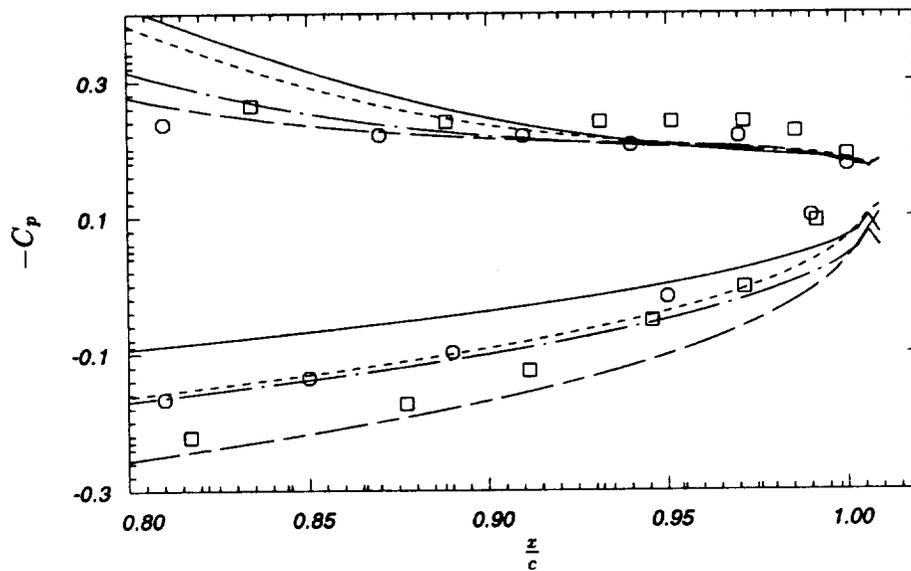

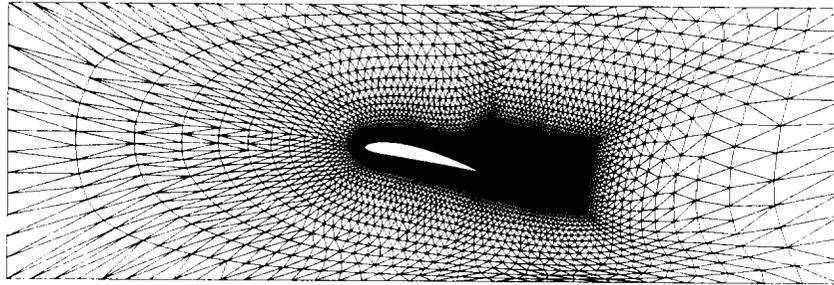FIGURE 10.   Closeup of the trailing-edge region (same legend as above).

FIGURE 11. The crosssectional plane of an unstructured mesh which accounts for the inviscid effects of the wind tunnel walls.

order methods will have a more complete representation of the residual error of the discrete approximation and, therefore, the scheme will be less dissipative. Second, alternative filters, described in Jansen (1994), can be implemented and tested. It is difficult to predict at this time if the method will lose computational efficiency when extended to higher order.

3.4 Expanded spanwise domain

Once we are satisfied with the solution in the region of the nose, we will have to consider carefully the effect of the narrow spanwise domain on our solution. It is likely that as we predict a larger separation at the trailing edge, the effect of the narrow domain will become more acute. Strategies are being developed to expand only the portion of the domain suffering from a narrow box. If these strategies work a large number of points can be saved.

REFERENCES

CHAPMAN, D. R. 1979 Computational aerodynamics development and outlook. *AIAA J.* **17**, 1293.

COLES, D., & WADCOCK, A. J. 1979 A flying-hot-wire study of two-dimensional mean flow past an NACA 4412 airfoil at maximum lift. *AIAA J.* **17**, 321.

HASTINGS, R. C.& WILLIAMS, B. R. 1987 Studies of the flow field near a NACA 4412 aerofoil at nearly maximum lift. *Aero. J.* **91**, 29.

JANSEN, K. 1994 Unstructured grid large eddy simulation of flow over an airfoil. *Annual Research Briefs 1994*. Center for Turbulence Research, NASA Ames/Stanford Univ.

JANSEN, K., JOHAN, Z., & HUGHES, T. J. R. 1993 Implementation of a one-equation turbulence model within a stabilized finite element formulation of a symmetric advective-diffusive system. *Comp Meth Appl Mech Eng.* **105**, 405.

JOHAN, Z., HUGHES, T. J. R., MATHUR, K. K., & JOHNSSON, S. L. 1992 A data parallel finite element method for computational fluid dynamics on the Connection Machine system. *Comp. Meth. Appl. Mech. Eng.* **99**, 113.

MENTER, F. R. 1994 Two-equation eddy-viscosity turbulence models for engineering applications. *AIAA J.* **32-8**, 1598-1605.

ROGERS, S. E., & KWAK, D. 1991 An upwind differencing scheme for the steady-state incompressible Navier-Stokes equations. *J. Appl. Num. Math.* **8**, 43-64.

WADCOCK, A. J. 1987 Investigation of low-speed turbulent separated flow around airfoils. *NACA CR 177450*.